of relaxation regimes for different concentrations at different temperatures. We find that in the low-temperature, slow-relaxation ($\omega_s\tau_s \gg 1$) regime, $\Gamma_B$ is approximately independent of angle. On the other hand, $\Gamma_B$ is quite angularly dependent in the high-temperature regime.

We have computed the spectra according to the expression given by Lin and Wang and have compared them with the experimental spectra. In this effort we have extracted the values of various parameters present in the theory. We have found proper angular dependences for $\omega_s$, $\tau_s$, $k_{22}(0)$, and $\alpha_3'$ as a function of concentration. The values determined for these parameters are shown to behave in a physically meaningful way, indicating that the basic principles inherent in the generalized hydrodynamic theory are reasonable.

**Acknowledgment.** We acknowledge the National Science Foundation, Polymers Program (Grant No. DMR79-12457), for providing financial support for this research.

## References and Notes

(1) Montrose, C. J.; Litovitz, T. A. *J. Acoust. Soc. Am.* **1970** *42*, 1250.
(2) Demoulin, C.; Montrose, C. J.; Ostsowsky, N. *Phys. Rev. A* **1974**, *9*, 1740.
(3) Montrose, C. J.; Solovyev, V. A.; Litovitz, T. A. *J. Acoust. Soc. Am.* **1968**, *43*, 117.
(4) Huang, Y. Y.; Wang, C. H. *J. Chem. Phys.* **1974**, *61*, 1868.
(5) Isakovich, M. A.; Chaban, I. A. *Sov. Phys. JETP* **1965**, *23*, 893.
(6) Wang, C. H.; Huang, Y. Y. *J. Chem. Phys.* **1976**, *64*, 4847.
(7) Wang, C. H.; Lin, Y.-H.; Jones, D. R. *Mol. Phys.* **1979**, *37*, 287.
(8) Lin, Y.-H.; Wang, C. H. *J. Chem. Phys.* **1978**, *69*, 1101.
(9) Lin, Y.-H.; Wang, C. H. *J. Chem. Phys.* **1979**, *70*, 681.
(10) Fytas, G.; Lin, Y.-H.; Chu, B. *J. Chem. Phys.* **1981**, *74*, 3131.
(11) Lempert, Walter; Wang, C. H. *J. Chem. Phys.* **1980**, *72*, 2570.
(12) Lempert, Walter; Wang, C. H., to be published.
(13) Boundy, R. H., Ed. "Styrene, Its Polymers, Copolymers, and Derivatives", Reinhold: New York, 1952.
(14) Mori, H. *Prog. Theor. Phys. (Kyoto)* **1964**, *33*, 1123.
(15) Mori, H. *Prog. Theor. Phys. (Kyoto)* **1965**, *34*, 399.
(16) Brody, E. M.; Lubell, C. J.; Beatty, C. L. *J. Polym. Sci., Polym. Phys. Ed.* **1975**, *13*, 295.
(17) Berne, B. J.; Pecora, R. "Dynamic Light Scattering"; Wiley: New York, 1976; Chapter 10.

# Light Scattering and Spectroscopic Studies of Polymerization Processes. 2. Thermal Polymerization of Styrene

**Benjamin Thomas Peng-Nien Chu* and Georg Fytas**

*Chemistry Department, State University of New York at Stony Brook, Long Island, New York 11794.* *Received September 9, 1981*

ABSTRACT: By using the thermal polymerization of styrene as an illustration, we propose a scheme which utilizes Raman spectroscopy and light scattering as probes for concentration, molecular weight, and size determinations in specific polymerization processes. Raman-active lines for polymer and monomer can be used to monitor the respective concentrations while the osmotic compressibility, $(\partial\pi/\partial C)_{T,P}$, and the Rayleigh ratio, $R_{vv}(K)$, can be related to the molecular weight of the polymer empirically even at very high polymer solution concentrations. In addition, we have studied static and dynamic properties of polystyrene in cumene and in styrene in dilute solutions in order to ascertain the general behavior of polystyrene dissolved in its own monomer, styrene.

## I. Introduction

Studies of polymerization processes have been difficult because we lack a convenient probe which can measure *on line* the concentrations of the monomer(s) and of the polymer in a polymerization reaction. Spectroscopic techniques such as NMR, IR, Raman, and fluorescence spectroscopy and other physical methods such as density and surface tension measurements offer reasonable and possible alternatives which permit us to monitor the appropriate concentration changes in chemical reactions. However, in a polymerization process, we really want to know not only the concentrations of the monomer ($C_m$) and/or of the polymer ($C_p$) but also the molecular weight ($M$) of the polymer during the reaction. In the present article, we demonstrate that it is feasible to devise a scheme which can accomplish the above goals, i.e., the determination of $C_p$ and/or $C_m$ and $M$ as a function of time for specific polymerization processes. In particular, we plan to devote our attention to studies of the thermal polymerization of styrene, including light scattering measurements of polystyrene in cumene and in its own monomer, styrene.

Light scattering intensity measurements can be used to determine the molecular weight, the second virial coefficient ($A_2$), and the radius of gyration ($r_g$) in very dilute solutions. At higher polymer concentrations we propose to take advantage of our understanding of the scaling concept[1] which will permit us to establish an empirical relationship between light scattering intensities and the molecular weight as well as the correlation length $\xi$ as a function of $M$ and $C_p$. In a later article, we shall also examine the molecular weight distribution[2] (MWD) and pseudogel formation using Rayleigh line width measurements and correlation function profile analysis.[3]

It should be emphasized that we are interested mainly in the application of light scattering intensity and spectroscopic techniques to study polymerization reactions and in the development of a practical *concentration* and *molecular weight* probe for polymerization process control. We are concerned with utilizing our knowledge of light scattering in the semidilute regime and of Raman spectroscopy as probes which will permit us to examine polymerization kinetics *on line*, based on sound fundamental principles. An outline of this work was presented as an invited lecture at the Symposium on Applications of Spectroscopy to Problems in Polymer Engineering and Science in the 1981 Spring National Meeting of the American Institute of Chemical Engineers, Houston, Texas.

## II. Theoretical Rationale

**1. Raman Spectroscopy.** Raman spectroscopy has been a useful tool to elucidate the structure of polymers. On occasion, it has been used to determine concentrations

0024-9297/82/2215-0561$01.25/0 

of monomer sequences in copolymers.[4] In a chemical reaction, some bonds are usually broken and others are being formed while most remain relatively unchanged. Therefore, Raman peaks which are characteristic of the respective chemicals of interest can be used to monitor the concentrations of those chemicals. As our ultimate aim is to design and to construct a probe which can be used in polymerization process control, we take advantage of a reference peak whose Raman intensity remains relatively constant during the chemical reaction. In the present article, we want to use Raman spectra for concentration determination of specific species during the reaction and not for structure investigations. Consequently, in the final probe design, a fairly low-resolution spectrometer for measuring the appropriate Raman peaks is likely to suffice.

**2. Intensity of Scattered Light.** In dilute solutions, at finite scattering angles and finite concentrations, we have

$$\frac{HC}{R_{vv}(K)} = \left(\frac{1}{M_w}\ \frac{1}{P(K)}\right) + 2A_2C + ... \qquad (1)$$

where $H$ [$=(\partial n/\partial C)_{T,P}4\pi^2n^2/N_A\lambda_0$] is a constant dependent upon the refractive index increment $(\partial n/\partial C)_{T,P}$ and the wavelength of the incident light in the medium $\lambda$ ($=\lambda_0/n$), $C$ is the concentration expressed in g/cm$^3$, and $M_w$ and $A_2$ are, respectively, the weight-average molecular weight and the second virial coefficient. $R_{vv}(K)$ is the excess Rayleigh ratio due to concentration fluctuations of the polymer solution using vertically polarized incident and scattered light and $P(K)$ is the particle scattering factor. Light scattering has been a standard technique for the determination of $M_w$, $A_2$, and the radius of gyration, $r_g$.

**a. Absolute Scattered Intensity.** Equation 1 is no longer valid at higher concentrations. Now we want to stress that although we cannot yet devise a quantitative theoretical expression which will relate $HC/R_{vv}(K)$ to the molecular weight at high concentrations, we can obtain a unique and empirical relationship between $\lim_{K\to 0} HC/R_{vv}(K)$ and the molecular weight over a range of concentrations up to semidilute solutions. As we can always write

$$\lim_{K\to 0} \frac{HC}{R_{vv}(K)} = \frac{(\partial\pi/\partial C^v)_{T,P}}{RT} \qquad (2)$$

where $K$ [$=(4\pi/\lambda)\sin(\theta/2)$] is the magnitude of the momentum transfer vector, the osmotic compressibility value at fairly high concentrations can be related to the molecular weight, at least for monodisperse systems. The superscript $v$ is used to emphasize the concentration unit to be g/cm$^3$.

**b. Angular Distribution of Scattered Intensity, $R_{vv}(K)$.** The characteristic length $L$ can be computed with the relation

$$R_{vv}(K) = R_{vv}(0)/(1 + L^2K^2/3) \qquad (3)$$

At infinite dilution, $L^2 = \langle r_g^2\rangle_z$. In the semidilute regime, $L$ is related to a correlation length $\xi$.

**3. Spectrum of Scattered Light,[5] $I(K,\omega)$.** The measured single-clipped photocount autocorrelation function has the form

$$G^{(2)}{}_k(\tau) = A(1 + b|g^{(1)}(\tau)|^2) \qquad (4)$$

where $k$ is the clipping level, $A$ is the background, and $b$ is an unknown parameter in the data-fitting procedure. $\tau$ ($=I\Delta\tau$) is the delay time, with $I$ and $\Delta\tau$ being the channel number and the increment delay time, respectively. $g^{(1)}(\tau)$ is the normalized correlation function of the scattered electric field.

**a. Translational Diffusion Coefficient.**[6] For a monodisperse system of spherically symmetric and noninteracting macromolecules in solution (or colloidal particles in suspension)

$$(Ab)^{1/2}|g^{(1)}(K,\tau)| \propto I(K)e^{-DK^2\tau} \qquad (5)$$

where the total scattered intensity $I(K) = Ni(K)$, with $N$ and $i$ being the number of macromolecules in the scattering volume $V$ and the scattered intensity from each macromolecule, respectively. $D$ is the translational diffusion coefficient. At finite but dilute concentrations and in the presence of interactions

$$D = D_0(1 + k_DC + ...) \qquad (6)$$

where $D_0$ ($=k_BT/f_0$) is the diffusion coefficient at infinite dilution, with $k_B$ and $f_0$ denoting the Boltzmann constant and the frictional coefficient at infinite dilution. The hydrodynamic and thermodynamic factors are combined in $k_D$ as

$$k_D = 2A_2M - k_f - N_AV_1/M \qquad (7)$$

where $k_f$ is the first-order friction coefficient and $\bar{v}$ ($=N_AV_1/M$) is the specific volume of the polymer, with $V_1$ being the polymer molecular volume. We shall discuss the dynamic properties of polystyrene in cumene and in styrene in dilute solutions and defer the utilization of the concentrated-solution behavior for MWD studies till a later article.

**b. Correlation Function Profile Analysis.**[7-9] For a polydisperse sample

$$|g^{(1)}(\tau)| = \int_0^\infty G(\Gamma)\exp(-\Gamma\tau)\,d\Gamma \qquad (8)$$

where $G(\Gamma)$ is the normalized distribution of decay rates. As we cannot obtain $G(\Gamma)$ precisely using the Laplace inversion, we can approximate $G(\Gamma)$ by computing its moments (or cumulants) by using a Pearson distribution function and by using a histogram method. In the cumulants method,[7] the average line width $\bar{\Gamma}$ is defined as

$$\bar{\Gamma} = \int G(\Gamma)\Gamma\,d\Gamma \qquad (9)$$

and the moments are defined as

$$\mu_i = \int (\Gamma - \bar{\Gamma})^iG(\Gamma)\,d\Gamma \qquad (10)$$

with $\mu_2/\bar{\Gamma}^2$ as the variance.

**4. Scaling Concept.**[1] The scaling theories have been quite successful in describing the static and dynamic properties of polymer solutions,[3,6,10,11] especially in the limit $N \to \infty$, where $N$ is the number of monomers per chain. Experiments on both static and dynamic properties of polymer solutions have shown reasonable agreement with predictions of the scaling laws. For example, in dilute solution, $L$ ($\equiv\langle r_g^2\rangle_z^{1/2}$) can be scaled as

$$L \propto N^\nu\tau^r \qquad (11)$$

where $N$ is the equivalent number of links in the statistical chain, $\tau$ [$\equiv(T-\Theta)/\Theta$] is the reduced temperature distance from the theta ($\Theta$) temperature, and $r = 2\nu - 1$. For the osmotic compressibility

$$(\partial\pi/\partial C^v)_{T,P} \propto C^{\sim 0} \qquad (12)$$

where the small slope is governed by the magnitude of $A_2$ as expressed according to eq 1. In the semidilute region

$$(\partial\pi/\partial C^v)_{T,P}/T \propto \frac{1}{N}(C/C^*)^m \quad \text{or} \quad \tau^nC^m \qquad (13)$$

where $C^*$ is the overlap concentration, $m = 1/(3\nu - 1)$, and

$n = 3r/(3\nu - 1)$. Thus in a good solvent where $\nu = {}^3/_5$, $m = {}^5/_4$, or $(\partial\pi/\partial C^v)_{T,P} \propto C^{5/4}$. There are many relations which can be predicted by the scaling concept. Although the scaling concept does not predict the curve shape in a transition region for the concentration dependence of the osmotic compressibility from dilute to semidilute solutions, the emphasis here is to state that the osmotic compressibility for a specific system has a unique value as a function of $T$, $M$, and $C$. Furthermore, the shape of $(\partial\pi/\partial C^v)_{T,P}$ vs. $C$ can be represented by typical curves as shown in Figure 2 of ref 12, Figure 8 of ref 6, and Figure 1 of ref 13 for dilute and semidilute solutions of polystyrene in *trans*-decalin. In our applications, we should avoid measurements near the critical region as demonstrated by the 20 °C isotherm in Figure 1 of ref 13, where an anomaly near the overlap concentration $C^*$ in the $(\partial\pi/\partial C)_{T,P}$ vs. concentration plot has been observed. Aside from the critical anomaly, the shape of the curve remains essentially the same using different molecular weights and solvents as can be demonstrated in a plot of log $(\partial\pi/\partial C^v)/T$ vs. log $C/C^*$. Although we cannot yet compute $(\partial\pi/\partial C^v)_{T,P}$ based on our knowledge of $M$, solvent quality, temperature, and concentration, we can predict the general shape of $(\partial\pi/\partial C^v)_{T,P}$ as a function of $M$, $C$, and $T$ and calibrate such curves empirically. It should be noted that for specific systems of known molecular weight distributions, we can calibrate the osmotic compressibility $(\partial\pi/\partial C^v)_{T,P}$ as a function of concentration at constant temperatures to about the same precision as light scattering intensity measurements in dilute polymer solutions. An interesting and fortunate compensating factor is that while in dilute solutions, we cannot determine the concentration with the same percentage of precision as in semidilute solutions, the concentration dependence of $(\partial\pi/\partial C^v)_{T,P}$ is weak. On the other hand, at higher concentrations, while we are dealing with relatively steep curves of $(\partial\pi/\partial C^v)_{T,P}$ as a function of concentration, we can determine the concentration to about 0.2%, depending upon the nature of the Raman peaks.

## III. Central Ideas of the Technique

The central ideas of the technique are to use (1) Raman spectra to measure the concentrations of the monomer and of the polymer, (2) the Rayleigh ratio $R_{vv}(K)$ and/or the osmotic compressibility $(\partial\pi/\partial C^v)_{T,P}$ to measure the molecular weight of the polymer, and eventually (3) dynamic light scattering to estimate the polydispersity effects and pseudogel motions. As Raman scattering and light scattering are complementary techniques, we can use essentially the same instrumentation.

**1. Concentration of Species Based on Raman Spectra.** The principle of the method is to record Raman spectra from the sample at different stages of polymerization. Study of thermal polymerization of styrene by Raman scattering has been reported.[14]

In a polymerization reaction some portion of the molecular structure of interest usually remains unchanged. The corresponding Raman-active lines are present throughout the process and can be used as standards to calibrate the intensity of other lines, while those related specifically to the monomer vanish and those related to the polymer grow. Monitoring a ratio of intensities makes the measurements insensitive to laser power fluctuations or sample turbidity. In particular, applications of the method for studying *copolymerization processes* should be a worthwhile extension.

**2. Molecular Weight of Polymer from Osmotic Compressibility and/or Rayleigh Ratio.** From discussions in section II, we see that at constant temperature

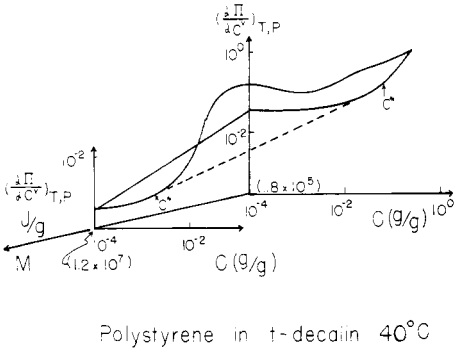


**Figure 1.** Schematic representation of a three-dimensional plot of the osmotic compressibility as a function of molecular weight and concentration for polystyrene in *trans*-decalin at 40 °C using data in ref 6 and 13. $C^*$ is the overlap concentration. As $\lim_{C\to0}(\partial\pi/\partial C^v)_{T,P}/RT = 1/M_w$, we have the osmotic compressibility proportional to the reciprocal of the weight-average molecular weight at infinite dilution and monotonic in $M$ whenever $A_2$ is positive. The wiggle in Figure 1 between the two $(\partial\pi/\partial C^v)_{T,P}$ vs. $C$ curves at $M = 1.8 \times 10^5$ and $1.2 \times 10^7$ symbolizes a cut of the $(\partial\pi/\partial C^v)_{T,P}$–$M$–$C$ surface. It does not mean that $(\partial\pi/\partial C^v)_{T,P}$ is *not* monotonic in $M$.

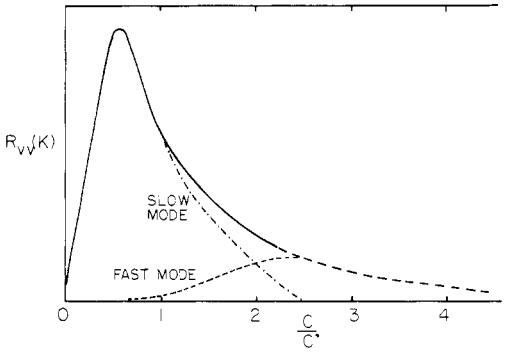


**Figure 2.** Schematic representation of $R_{vv}(K)$ as a function of reduced concentration $(C/C^*)$ for polystyrene in a Θ solvent using data in ref 6 and 15.

we can produce a unique surface in the $(\partial\pi/\partial C^v)_{T,P}$–$C_p$–$M$ three-dimensional plot for a specific polymerization reaction. Figure 1 shows a schematic plot of $(\partial\pi/\partial C^v)_{T,P}$ vs. $C_p$ and $M$ for polystyrene in *trans*-decalin at 40 °C. It is quite clear that we can create such a surface for a specific polymerization process such as the polystyrene in styrene system. Furthermore, the temperature dependence of such a surface can be estimated if we know, for example, how $A_2$ and $r_g$ change as a function of temperature.

The important point is that we have illustrated the feasibility of using $(\partial\pi/\partial C^v)_{T,P}$ to provide a determination of $M$ at fairly high concentrations in the semidilute regime by combining Raman and light scattering intensity measurements and by taking advantage of the scaling concept which assures us that there are no surprises in the $(\partial\pi/\partial C^v)_{T,P}$–$C_p$–$M$ surface, where $C_p$ denotes the polymer concentration. Thus we can determine $M$ from $(\partial\pi/\partial C^v)_{T,P}$ and $C_p$ up to very high concentrations (~50 wt % polymer) for $M \sim 10^5$. In fact, the functional form of $(\partial\pi/\partial C^v)_{T,P}[C_p,M]$ can also be estimated by mean-field theories.

In determining $(\partial\pi/\partial C^v)_{T,P}$, we have to extrapolate $R_{vv}(K)$ to $K = 0$. This procedure may prove to be tedious in reality. Here we suggest an alternative by examining $R_{vv}(K)$ at some fixed $K$. At finite $K$, the Rayleigh ratio $R_{vv}(K)$ contains information on $(\partial\pi/\partial C^v)_{T,P}$ and $L$. As eq 1 is valid only in very dilute solutions, the relationship becomes complex at high concentrations. However, we are not concerned with the exact theoretical predictions. There is a unique relationship between $R_{vv}(K)$ and $C$ at

Table I
Values of Physical Constants for Cumene and Styrene

| | cumene | styrene [b] |
|---|---|---|
| density, [a] $\rho$ (g/cm$^3$) | $0.8788 - 8.5 \times 10^{-4} t$ °C | $0.9238 - 8.77 \times 10^{-4} t$ °C |
| refractive index, [a] $n_{488}$ | $1.5119 - 5.1 \times 10^{-4} t$ °C | $1.5748 - 5.18 \times 10^{-4} t$ °C |
| viscosity, $\eta$ (cP) | $0.01134 \times \exp(1273/T(\mathrm{K}))$ | $0.0119 \times \exp(1228/T(\mathrm{K}))$ |
| refractive index increment, $dn/dc$ | $0.581 - (n-1)/\rho$ | 0.046 |

[a] Timmermans, J. "Physicochemical Constants of Pure Organic Compounds"; Elsevier Publishing Co.: New York, 1965; Vol. II. [b] Boundy, R. H.; Boyer, R. F., Eds. "Styrene, Its Polymers, Copolymers, and Derivatives"; Hofner Publishing Co.: New York, 1952.

different molecular weights. Figure 2 shows a schematic plot of $R_{vv}(K)$ vs. concentration for a low molecular weight polystyrene ($M \sim 1.79 \times 10^5$) in a Θ solvent. The shape of the curve again shows a universal feature because $R_{vv}(K)$ should have a sharp increase at low concentrations, reach a maximum near $C/C^* \sim 1$, and approach zero at 100% polymer concentration. $R_{vv}(K)$ produces another unique surface in a three-dimensional $R_{vv}(K)$–$M$–$C^v$ (g/cm$^3$) plot.

## IV. Experimental Methods

The Raman spectrometer[14] has been modified to take a high-temperature cell for the thermal polymerization of styrene and to measure absolute light scattering intensity at four fixed scattering angles. The detailed design of the light scattering spectrometer has been described elsewhere.[16] We used an argon ion laser operating at 488.0 nm. Integrated intensities were measured by a standard photon-counting technique while the single-clipped photoelectron count autocorrelation function was measured with a Malvern K7023 correlator. Temperatures were controlled to ±0.01 °C near room temperature and to ±0.05 °C at high temperatures.

Two polystyrene samples were used for this investigation. One sample was an NBS 705 standard with $M_w = 1.79 \times 10^5$ and $M_z:M_w:M_n = 1.12:1.07:1$. The other one was purchased from Pressure Chemical Co. (lot no. 14a) and had $M_w = 1.8 \times 10^6$ and $M_w/M_n < 1.20$. The styrene fluid was degassed by several freeze–pump cycles, with the inhibitor (*tert*-butylpyrocatechol) being left undisturbed. Our results were independent of the presence of a small amount of the inhibitor.[14] All solutions were filtered through a Millipore filter of nominal pore diameter 0.22 μm before light scattering measurements.

## V. Results and Discussion

**1. Polystyrene in Cumene.** Light scattering intensity and line width measurements were performed for polystyrene (NBS 705 standard) in cumene as a function of concentration ($C = 7.03 \times 10^{-4}$, $1.845 \times 10^{-3}$, $4.049 \times 10^{-3}$, $9.530 \times 10^{-3}$, and $1.427 \times 10^{-2}$ g/g) at 25 and 40 °C over a range of scattering angles. We wanted to learn how polystyrene behaves in its own monomer, styrene. Cumene represents another solvent whose molecular structure resembles the polystyrene monomer unit. With information from benzene, toluene, cumene, styrene, cyclohexane, and methylcyclohexane, we try to gain a better insight into the relationship between solvent quality and its molecular structure for polystyrene solutions.

**a. Static Properties.** Values of physical constants for cumene are summarized in Table I. The Rayleigh ratio has been defined as

$$R_{vv} = \left( \frac{I_p - I_s}{I_B} \left( \frac{n_s}{n_B} \right)^2 \right) R_{vv}^B \equiv R_{vv}^* R_{vv}^B \qquad (14)$$

where $I_p$, $I_s$, and $I_B$ are the vv components of the scattered intensity for the polymer solution, the solvent, and the reference standard benzene, respectively. $n_s$ and $n_B$ are the refractive indexes of the solvent (cumene) and benzene, with $(n_s/n_B)^2$ being the correction factor for the change in the scattering volume due to refraction as seen by the photodetector. This correction factor depends upon the optical geometry of our light scattering instrument. $R_{vv}^B$ is the Rayleigh ratio for benzene. Figure 3 shows plots of $1/R_{vv}^*$ vs. $\sin^2(\theta/2)$. In dilute solution, the characteristic length $L$ can be identified with the apparent radius of gyration, which is related to $r_g$ at infinite dilution by means of the second virial coefficient $A_2$:

$$L^2 = \langle r_g^2(C^v = 0) \rangle_z / (1 + 2A_2 M C^v) \qquad (15)$$

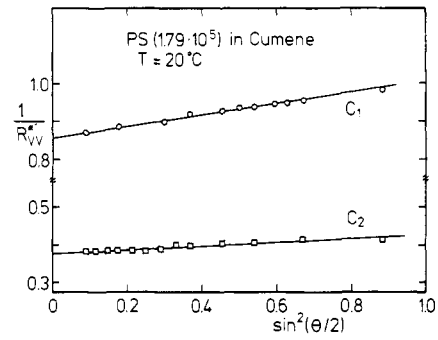


**Figure 3.** Plots of $1/R_{vv}^{*\prime}$ vs. $\sin^2(\theta/2)$ for polystyrene (NBS 705 standard) in cumene at $C_1 = 6.06 \times 10^{-4}$ g/cm$^3$ (denoted by hollow circles) and $C_2 = 1.59 \times 10^{-3}$ g/cm$^3$ (denoted by hollow squares) at 20 °C.

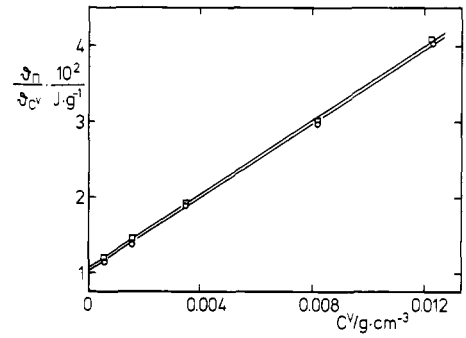


**Figure 4.** Plots of $(\partial\pi/\partial C^v)_{T,P}$ vs. concentration for polystyrene (NBS 705 standard) in cumene at 20 °C (hollow circles) and 40 °C (hollow squares).

Figure 4 shows plots of the osmotic compressibility $(\partial\pi/\partial C^v)_{T,P}$ as a function of concentration at 20 and 40 °C. The straight-line behavior tries to stress the point that in the dilute-solution region, $(\partial\pi/\partial C^v)_{T,P}$ is proportional to $C^{\sim 0}$, as $A_2$ is quite small. We can compute $L$, $A_2$, and $r_g$ according to eq 1, 3, and 15. Furthermore, the polymer solution behaves normally as a dilute solution with a positive $A_2$. Table II lists values of $L$, $A_2$, and $L(1 + 2A_2MC^v)^{1/2}$, where we have used a molecular weight of $2.2 \times 10^5$ as determined independently by our light scattering experiments at two different temperatures. The $2.2 \times 10^5$ value is much higher than we have anticipated. However, our results are internally consistent. Over a 20 °C change in temperature, we cannot yet be certain whether $A_2$ increases or decreases with increasing temperature. The absolute excess scattered intensity at $C = 1.427 \times 10^{-2}$ g/g and $\theta = 35°$ was measured at 20, 40, and 70 °C. After correction for $L$, we have determined that the second virial coefficient $A_2$ decreases with increasing temperature, as shown in Figure 5. The negative temperature coefficient for $A_2$ implies that the solvent quality decreases with increasing temperature.

Table II
Values of Apparent Characteristic Length $L$, Second Virial Coefficient $A_2$, and Radius of Gyration $r_g$ for Polystyrene (NBS 705 Standard) in Cumene

| temp, °C | concn, g/cm³ | $L$, Å | $A_2$, (cm³ mol)/g² | $L(1 + 2A_2MC^v)^{1/2}$, [a] Å |
|---|---|---|---|---|
| 20 | $6.06 \times 10^{-4}$ | 170 | $4.9 \times 10^{-4}$ | 181 |
| 20 | $1.59 \times 10^{-3}$ | 155 | $4.9 \times 10^{-4}$ | 180 |
| 20 | infinite dilution | 180 (by extrapolation) | | 181 |
| 40 | $6.06 \times 10^{-4}$ | 175 | $4.7 \times 10^{-4}$ | 186 |
| 40 | $1.59 \times 10^{-3}$ | 154 | $4.7 \times 10^{-4}$ | (178) |
| 40 | infinite dilution | 190 (by extrapolation) | | 188 |

[a] Equation 15.

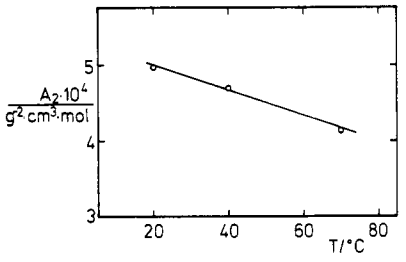


**Figure 5.** Plot of $A_2$ vs. temperature for polystyrene (NBS 705 standard) in cumene.

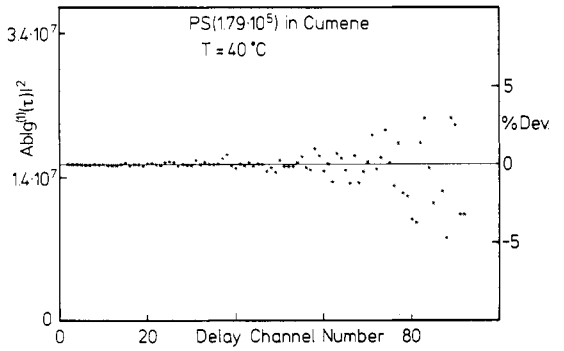


**Figure 6.** Plot of $Ab|g^{(1)}(\tau)|^2$ vs. delay channel number $I$ for polystyrene (NBS 705 standard) in cumene at $C = 9.53 \times 10^{-3}$ g/g, $\theta = 35°$, $t = 40$ °C, and $\Delta\tau = 5.1$ μs, with $\tau = I\Delta\tau$. By fitting $(Ab)^{1/2}|g^{(1)}(\tau)|$ to $(Ab)^{1/2}\exp(-\bar{\Gamma}\tau + \mu_2\tau^2/2)$, we obtained $\bar{\Gamma} = 5.32 \times 10^3$ rad/s and $\mu_2/\bar{\Gamma}^2 = 0.039$ with $A = 1.244 \times 10^8$ and $b|g^{(1)}(\Delta\tau)|^2 = 0.28$.

**b. Dynamic Properties.** Figure 6 shows a typical plot of the net autocorrelation function $Ab|g^{(1)}(\tau)|^2$ as a function of delay channel number $I$ for $C = 9.53 \times 10^{-3}$ g/g at $\theta = 35°$, $t = 40$ °C, and $\Delta\tau = 5.1$ μs. We have used the cumulants method[7] (eq 9 and 10 and up to second order) to fit the experimental correlation function using the fitting parameters $Ab$, $\bar{\Gamma}$, and $\mu_2$. In all the solutions measured in this system, $\mu_2/\bar{\Gamma}^2 \sim 0.02$–$0.05$. No systematic deviation was observed, as shown in Figure 6 by using the cumulants fit with

$$y = Ab|g^{(1)}(\tau)|^2 = Ab\exp(-2\bar{\Gamma}\tau + \mu_2\tau^2) \qquad (16)$$

where % dev = $100(y_{\text{measd}} - y(\text{eq } 16))/y(\text{eq } 16)$. Figure 7 shows plots of $\bar{D}$ $(=\bar{\Gamma}/K^2)$ vs. concentration at 20 °C (hollow circles) and 40 °C (hollow squares). According to eq 6, we obtained

$$\bar{D}_{20} = 2.51 \times 10^{-7}(1 + 23.8C^v) \text{ cm}^2/\text{s} \qquad (17)$$

$$\bar{D}_{40} = 3.26 \times 10^{-7}(1 + 29.7C^v) \text{ cm}^2/\text{s} \qquad (18)$$

with $C^v$ expressed in g/cm³. Table III lists values of various parameters for polystyrene in cumene. The ratio $r_h/r_g$ is relatively constant over the 20 °C temperature change and has a value close to that for a good solvent. The polymer

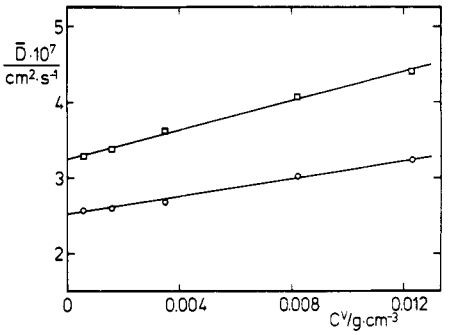


**Figure 7.** Plots of $\bar{D}$ $(=\bar{\Gamma}/K^2)$ vs. concentration for polystyrene (NBS 705 standard) in cumene at 20 °C (hollow circles) and 40 °C (hollow squares).

Table III
Values of Parameters for Polystyrene (NBS 705 Standard) in Cumene

| | temp, °C | |
|---|---|---|
| | 20 | 40 |
| $\bar{D}^0$, cm²/s × $10^{-7}$ | 2.51 | 3.26 |
| $\bar{f}^0 \equiv k_BT/\bar{D}^0$, g/s × $10^{-7}$ | 1.61 | 1.33 |
| $r_h \equiv k_BT/6\pi\eta_s\bar{D}^0$, Å | 98 | 107 |
| $r_g$, Å | 180 | 188 |
| $r_h/r_g$ | 0.54 | 0.57 |
| $k_D$, cm³/g | 23.8 | 29.7 |
| $k_f$, [a] cm³/g | 119 | 113 |

[a] $\bar{f} = [M(1 - \bar{v}C^v)/DN_A](\partial\pi/\partial C^v)_{T,P} = \bar{f}^0(1 + k_fC)$.[6]

dimension is larger in cumene than in *trans*-decalin,[6] which is a Θ solvent at room temperature, with an upper Θ temperature of 20.5 °C.

**2. Polystyrene in Styrene.** Light scattering intensity and line width measurements were performed for two polystyrene samples (polymer A: NBS 705 standard, with $M_w \sim 1.8 \times 10^5$; polymer B: Pressure Chemical Co., with $M_w \sim 1.8 \times 10^6$) over a range of concentrations and temperatures.

**a. Static Properties.** Values of physical constants for styrene are summarized in Table I. The refractive index increment for polystyrene in styrene is fairly small. With $dn/dc \sim 0.046$, the scattered intensity for dilute solutions of polystyrene in styrene is relatively weak. Therefore, we have not been able to obtain a reasonable estimate of the radius of gyration for the low molecular weight polystyrene (polymer A) in styrene. Nevertheless, it was surprising to learn that the polymer coil was quite contracted, leaving only a small angular dissymmetry. Figure 8 shows plots of the osmotic compressibility vs. concentration for polystyrene (NBS 705 standard) in styrene at 15.2 and 40 °C. Values of $A_2$ and $M_w$ are summarized in Table IV. Again, we obtained a molecular weight exceeding $2 \times 10^5$ while the reference value is $1.8 \times 10^5$. It should also be noted

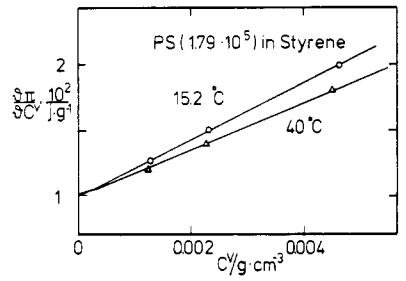


**Figure 8.** Plots of $(\partial\pi/\partial C^v)_{T,P}$ vs. concentration for polystyrene (NBS 705 standard) in styrene at 15.2 °C (hollow circles) and 40 °C (hollow triangles). The two curves cross each other near the zero concentration limit because $A_2$ decreases with increasing temperature. In a plot of $(\partial\pi/\partial C^v)_{T,P}/RT$ vs. $C^v$, the two curves would meet at $C = 0$.

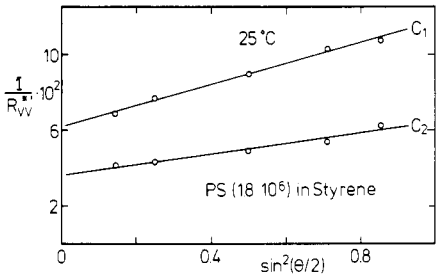


**Figure 9.** Plots of $1/R_{vv}^{*\prime}$ vs. $\sin^2(\theta/2)$ for polystyrene (polymer B, $M_w \sim 1.8 \times 10^6$) in styrene at 25 °C. $C_1 = 4.87 \times 10^{-4}$ g/cm³ and $C_2 = 1.04 \times 10^{-3}$ g/cm³.

Table IV
Values of Parameters for Polystyrene in Styrene

Polymer A: NBS 705 Standard, $M_w = 1.79 \times 10^5$

| | temp, °C | | |
|---|---|---|---|
| | 15.2 | 25 | 40 |
| $H$, (cm² mol)/g² × $10^{-8}$ | 6.0 | 5.97 | 5.91 |
| $A_2$, (cm² mol)/g² × $10^{-4}$ | 4.5 | 4.2 | 3.7 |
| $M_w \times 10^5$ | 2.4 | 2.4 | 2.6 |

Polymer B: Pressure Chemical Co., $M_w = 1.8 \times 10^6$ [a]

| | concn, g/cm³ × $10^{-4}$ | | |
|---|---|---|---|
| | infinite dilution | 4.87 | 10.41 |
| $L$, Å | 434 | 409 | 379 |
| $L(1 + A_2MC^v)^{1/2}$, Å | 471 | 463 | 480 |
| $A_2$, (cm² mol)/g² × $10^{-4}$ | | 1.7 | |
| $M_w \times 10^6$ | | 1.7 | |

[a] Parameters at 25 °C.

that $(\partial\pi/\partial C^v)_{T,P}$ at two different temperatures should be different at infinite dilution since $\lim_{C\to 0}(\partial\pi/\partial C^v)_{T,P}/RT = 1/M_w$. In addition, we should not take the difference between $2.4 \times 10^5$ and $1.8 \times 10^5$ literally as our determination of molecular weights is precise to about ±10%. It should also be noted that polystyrene in styrene is not stable because of thermal polymerization even at room temperatures. Therefore, we obtained a higher $M_w$ value in our determination of molecular weight of the NBS 705 polystyrene standard in styrene than in cumene. We conclude that *our* "NBS 705 standard" sample has a higher molecular weight. However, the results do not imply any lack of faith in the NBS standard. The only statement worthwhile mentioning here is that *our* present NBS sample seems to have a higher molecular weight even though its magnitude has no bearing on our objectives. In view of the small angular asymmetry observed for the NBS 705 standard polystyrene in styrene, we used a higher

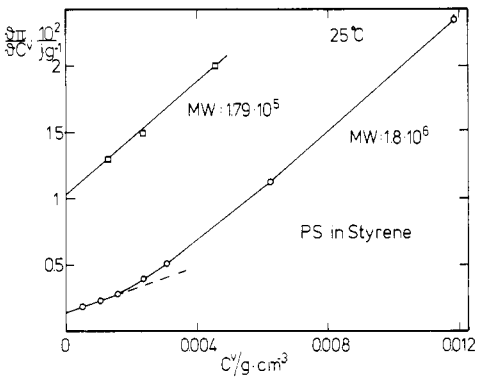


**Figure 10.** Plots of $(\partial\pi/\partial C^v)_{T,P}$ vs. concentration for polystyrene (polymers A and B) in styrene at 25 °C. The initial slope and the intercept of the lower curve yield $A_2 = 1.7 \times 10^{-4}$ (cm³ mol)/g² and $M_w = 1.7 \times 10^6$.

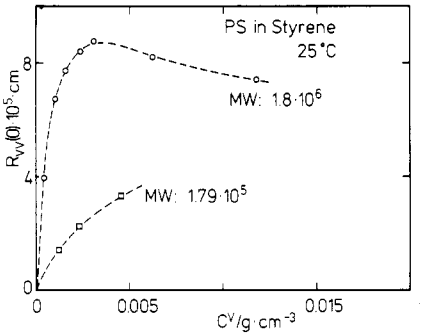


**Figure 11.** Plots of $R_{vv}(\theta = 45°)$ vs. $C^v$ for polystyrene in styrene at 25 °C.

molecular weight polystyrene (polymer B: $M_w \sim 1.8 \times 10^6$) for size determinations. Figure 9 shows plots of $1/R_{vv}^{*\prime}$ vs. $\sin^2(\theta/2)$ for polymer B in styrene at 25 °C, where $R_{vv}^{*\prime} = I_p - I_s$. Therefore we have

$$R_{vv}(K) = R_{vv}^{*\prime}(R_{vv}^{B}/I_B)(n_s/n_B)^2 \qquad (19)$$

i.e., $R_{vv} = 2.42 \times 10^{-6} R_{vv}^{*\prime}$ cm⁻¹. From the slope over intercept of the curves in Figure 9, we have computed the characteristic length as listed in Table IV. Figure 10 shows plots of $(\partial\pi/\partial C^v)_{T,P}$ vs. concentration at 25 °C for polystyrene of two different molecular weights (polymers A and B). From the initial slope and the intercept of the curve for polymer B, we obtained $A_2 = 1.7 \times 10^{-4}$ (cm³ mol)/g² and $M_w = 1.7 \times 10^6$. At higher concentrations, $(\partial\pi/\partial C^v)_{T,P}$ is no longer linear. It moves upward in the same manner as exhibited by the schematic representation of Figure 1, based on data for polystyrene in a Θ solvent, *trans*-decalin. In Figure 10, the upward curvature appears to start at about the same concentration as polystyrene in *trans*-decalin because styrene turns out to be a fairly poor solvent for polystyrene. The polymer coil is more contracted than expected.

In determining the osmotic compressibility $(\partial\pi/\partial C^v)_{T,P}$, we have to extrapolate the absolute scattered intensity to zero scattering angle. We want to construct a $(\partial\pi/\partial C^v)_{T,P}$–$C_p$–$M$ surface in order to determine the molecular weight from measurements of $(\partial\pi/\partial C)_{T,P}$ and $C_p$. There is an alternative empirical approach which will permit us to determine the molecular weight without extrapolating the absolute scattered intensity to zero scattering angle; i.e., we can construct a $R_{vv}(K)$–$C_p$–$M$ surface as shown schematically in Figure 12. Again, the surface is not parallel to the $R_{vv}$–$C^v$, $R_{vv}$–$M$, and $M$–$C^v$ planes as the location and the magnitude of the maximum in $R_{vv}$–$C^v$ depend on the molecular weight. If we know $R_{vv}$ and $C^v$, the line with fixed $R_{vv}$ and $C^v$ values should intersect the

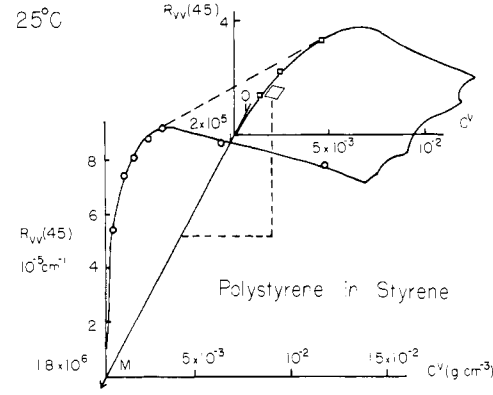


**Figure 12.** Schematic representation of a three-dimensional plot of the Rayleigh ratio $R_{vv}(\theta = 45°)$ as a function of molecular weight and concentration for polystyrene in styrene at 25 °C using data of Figure 11.

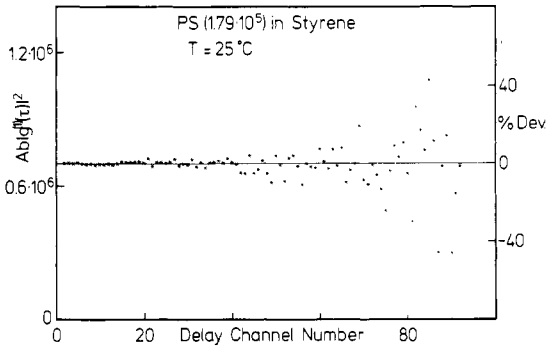


**Figure 13.** Plot of $Ab|g^{(1)}(\tau)|^2$ vs. delay channel number $I$ for polystyrene (NBS 705 standard) in styrene at $C = 5.04 \times 10^{-3}$ g/g, $\theta = 35°$, $t = 25$ °C, and $\Delta\tau = 6.4$ μs. By using the cumulants method, $\bar{\Gamma} = 4.80 \times 10^3$ rad/s and $\mu_2/\bar{\Gamma}^2 \sim 0.13$.

$R_{vv}$–$C^v$–$M$ surface at one point whose coordinate on the molecular weight axis is the molecular weight of the sample we want to find. Therefore, if the $R_{vv}(K)$–$C_p$–$M$ surface is known, we can study the details of the polymerization kinetics. The surface can be represented by a set of parametric equations including the temperature dependence, although we have not yet worked out the most efficient ways of representing such a surface (or contour lines). In particular, while polystyrene is an easy system to work with and can be used as an illustration to demonstrate the scheme, its practical value is more limited. Consequently, we are using this approach to study the melt ring-opening thermal polymerization kinetics of hexachlorocyclotriphosphazene and shall present those findings in a later article.

**b. Dynamic Properties.** Figure 13 shows a typical plot of the net autocorrelation function $Ab|g^{(1)}(\tau)|^2$ as a function of delay channel number $I$ with $\tau = I\Delta\tau$ for $C = 5.04 \times 10^{-3}$ g/g, $\theta = 35°$, $t = 25$ °C, and $\Delta\tau = 6.4$ μs. By using the cumulants method to fit the experimental data, we obtained $\bar{\Gamma} = 4.80 \times 10^3$ rad/s and $\mu_2/\bar{\Gamma}^2 \sim 0.13$. With $A = 2.436 \times 10^7$, $b|g^{(1)}(\Delta\tau)|^2 = 0.056$. The variance for the NBS 705 standard polystyrene is much higher than that of the same polymer in cumene. Furthermore, the ratio of the first point of the net autocorrelation function to the base line ($A$) (~0.056) is much lower than 0.28 for the same polymer in cumene. Although the second-order cumulants fit can represent both solutions (PS in styrene and cumene) equally well as shown by the percent deviation plots of Figures 6 and 13, the variance is distinctly different. Additional measurements of the NBS 705 standard in styrene at other concentrations and temperatures confirm the high variance value, ranging from 0.13 to 0.31. Two factors may contribute to this effect. As the refractive index increment for polystyrene in styrene is low, the stray light plays a more important role in introducing a partial homodyning contribution which may have a negligible effect on $\bar{\Gamma}$ but increases the variance significantly. Secondly, the styrene monomer fluid may contain a small amount of polystyrene which will introduce an arbitrary broadening in the molecular weight distribution. As the bimodal character in the molecular weight distribution function contributes strongly to an increase in the value of the variance, it is not surprising to find a much larger $\mu_2/\bar{\Gamma}^2$ for polystyrene in styrene. Figure 14 shows plots of $\bar{D}$ ($\equiv\bar{\Gamma}/K^2$) vs. concentration for polystyrene (polymer A) in styrene at 15.2, 25, and 40 °C. Additional line width measurements were performed for polymer B in styrene at 25 °C as shown in Figure 15. Again the variance (~0.2) is higher than expected.

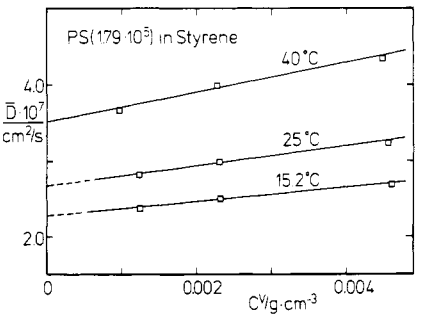


**Figure 14.** Plots of $\bar{D}$ ($\equiv\bar{\Gamma}/K^2$) vs. concentration for NBS 705 standard polystyrene in styrene at 15.2, 25, and 40 °C.

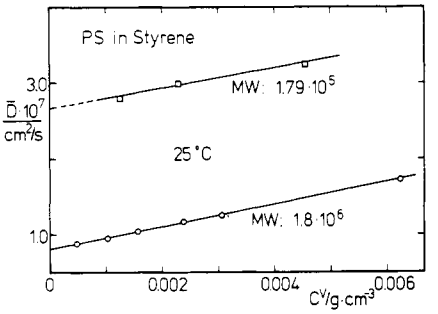


**Figure 15.** Plots of $\bar{D}$ ($\equiv\bar{\Gamma}/K^2$) vs. concentration for polystyrene (polymers A and B) in styrene at 25 °C.

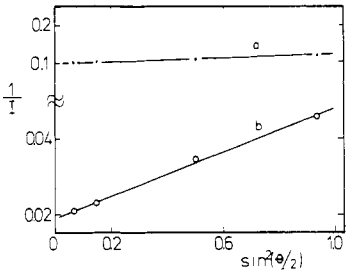


**Figure 16.** Plots of reciprocal relative scattered intensity vs. $\sin^2(\theta/2)$ for (a) a dilute solution of polystyrene (NBS 705 standard) in cyclohexane and (b) an aqueous suspension of 0.09-μm-diameter polystyrene latex spheres, both measured at 25 °C.

**3. Thermal Polymerization of Styrene.** In order to make simultaneous measurements of Raman scattering and light scattering at the four scattering angles, we first tested the stray light and the scattering volume corrections using a dilute solution of polystyrene (NBS 705 standard) in cyclohexane and an aqueous suspension of 0.09-μm-diameter polystyrene latex spheres as our references. Figure 16 shows plots of reciprocal relative scattered intensity vs. $\sin^2(\theta/2)$.

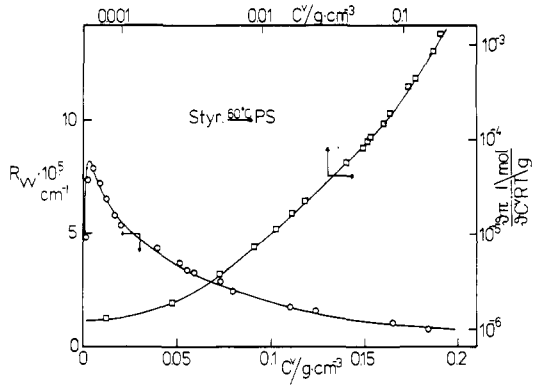


**Figure 17.** Plots of $R_{vv}$ and $(\partial\pi/\partial C^v)_{T,P}/RT$ vs. polystyrene concentration during the polymerization reaction at 60 °C.

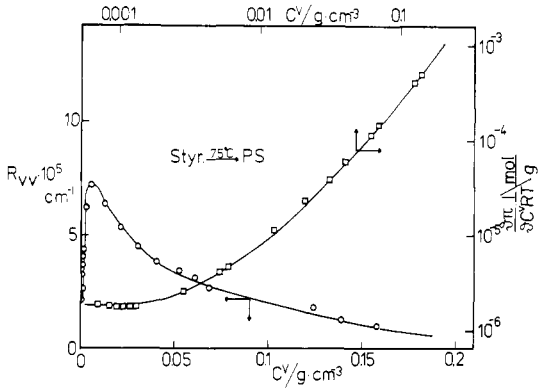


**Figure 18.** Plots of $R_{vv}$ and $(\partial\pi/\partial C^v)_{T,P}/RT$ vs. polystyrene concentration during the polymerization reaction at 75° C.

For the thermal polymerization of styrene at 60, 75, and 90 °C, no appreciable angular dissymmetry was detected. The Rayleigh ratio was computed according to

$$R_{vv}(K) = \frac{I_p - I_s}{I_B} R_{vv}^B \qquad (14a)$$

where we have neglected the refractive index correction and taken $I_s$ to be the initial scattered intensity of the styrene monomer. Only the mean $R_{vv}$ values from the four scattering angles at 30°, 45°, 90°, and 150° are presented. We ran two samples at each of the two temperatures 60 and 75 °C and found good reproducibility in our measurements. We used the same calibration on the ratio of the Raman intensities as a function of monomer concentration[14] in order to determine the amount of polymer (polystyrene) formed. Figures 17–19 show plots of $R_{vv}$ and $HC^v/R_{vv} \equiv (\partial\pi/\partial C^v)_{T,P}/RT$ vs. the polystyrene concentration during the polymerization reactions at 60, 75, and 90 °C, respectively.

The curves in Figures 17–19 are not necessarily cuts in the $R_{vv}$–$C_p$ and $(\partial\pi/\partial C^v)_{T,P}/RT$–$C_p$ planes at constant $M$. In fact, such cuts should be exceptions rather than the rule. Rather, the $R_{vv}$ vs. $C_p$ and the $(\partial\pi/\partial C^v)_{T,P}$ vs. $C_p$ curves are space curves on surfaces similar to those expressed schematically in Figures 1, 2, and 11, except that we have polystyrene in styrene at 60, 75, and 90 °C, respectively. Indeed, we intend to construct such surfaces for a more interesting polyphosphazene system to be presented in a future article. In the present work, let it suffice to say that the proposed scheme has been demonstrated. According to Figures 17–19, the intercept of $HC^v/R_{vv}$ (at $C^v = 0$) remains finite and we can determine the molecular weight of polystyrene during the initial polymerization process when the polymer concentration approaches infinite dilution. By using eq 1 and 2, we get $M_w = 8 \times 10^5$, $6 \times 10^5$, and $5 \times 10^5$ for polymerization temperatures at 60, 75, and 90 °C, respectively. In other words, the molecular weight, at least in the initial thermal polymerization process, increases with decreasing temperature, which for polystyrene is a well-known fact. In Figure 18, we have made additional measurements at concentrations below the overlap concentration $C^*$ and in the dilute-solution region. The horizontal slope displayed by the $(\partial\pi/\partial C^v)_{T,P}$ vs. the polystyrene concentration plot shows that, according to eq 1, the second virial coefficient $A_2$ is negligibly small, in good agreement with our polystyrene in styrene results, where we have intentionally dissolved known molecular weights of polystyrene in styrene. Although the temperature dependence of the second virial coefficient $A_2$ depends on the molecular weight, we know that polystyrene in styrene has reached the neighborhood of the lower Θ temperature ($\Theta_L$). It is interesting to predict that at higher temperatures ($T > \Theta_L$), polystyrene can be precipitated by its own monomer, styrene, because of the predicted existence of a coexistence curve with a lower critical mixing point. We should also note that in estimating $A_2$ in Figure 18 we have assumed a constant molecular weight while in fact such an assumption has to be proven by another independent experiment. Nevertheless, as we know that during the thermal polymerization of styrene the concentration of the polymer increases as a function of time and at low polymerization temperatures the molecular weight distribution of thermally polymerized polystyrene is quite narrow, the statement that $A_2$ is negligibly small near 75 °C for polystyrene in styrene is valid even though the results presented in Figures 17–19 are qualitative. For the $R_{vv}$ vs. $C^v$ plot, we note that at low concentrations $R_{vv}$ increases sharply for the lower polymerization temperatures, indicating a higher polystyrene molecular weight. The maximum for $R_{vv}$ as a function of $C^v$ also occurs at a lower polymer concentration, which confirms the conclusion that the average molecular weight of polystyrene increases with decreasing polymerization temperature. As $R_{vv}$ decreases and $(\partial\pi/\partial C)_{T,P}$ increases more sharply at higher concentrations ($C > C^*$), the system enters the semidilute and concentrated-solution regions.

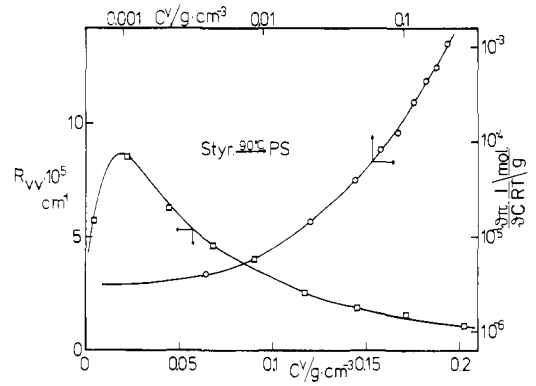


**Figure 19.** Plots of $R_{vv}$ and $(\partial\pi/\partial C^v)_{T,P}/RT$ vs. polystyrene concentration during the polymerization reaction at 90 °C.

A study of concentration fluctuations during the thermal polymerization of styrene using photon correlation spectroscopy has been reported by Patterson et al.[17] Here, we can combine photon correlation spectroscopy with classical light scattering and Raman scattering. We mention briefly that the analysis of the time correlation function using correlation function profile analysis from dilute to semidilute and concentrated-solution regions is more complex, involving separation of gel disentanglement motions of different coils and internal motions of individual coils from

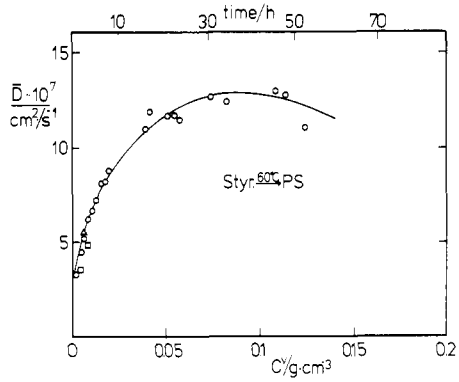


**Figure 20.** Plot of $\bar{D}$ ($\equiv\bar{\Gamma}/K^2$) vs. polymerization time and polystyrene concentration during the polymerization reaction at 60 °C and $\theta$ = 30° (hollow circles), 45° (hollow squares), and 90° (hollow triangles).

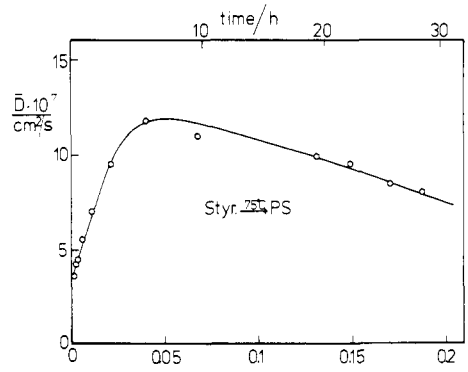


**Figure 21.** Plots of $\bar{D}$ ($\equiv\bar{\Gamma}/K^2$) vs. polymerization time and polystyrene concentration during the polymerization reaction at 75 °C.

the translational motions of the center of mass of each coil. In the present work, we present only the analysis by means of the cumulants method. Figures 20–22 show plots of $\bar{D}$ vs. polymerization time and polystyrene concentration for polystyrene in styrene during the thermal polymerization of styrene at 60, 75, and 90 °C, respectively.

By extrapolating $\bar{D}$ to zero concentration, we can compute the hydrodynamic radius of the polystyrene polymer during the initial polymerization process. With $r_h = kT/6\pi\eta_s\bar{D}$ and $\eta_s$ = 0.49, 0.40, and 0.34 cP, we get $r_h$ = 178, 170, and 165 Å at 60, 75, and 90 °C, respectively. By comparing the low $r_h$ and estimated $M_w$ values with our previous measurements of polystyrene (polymers A and B) in styrene, we can confirm that the initial molecular weights of polystyrene in the thermal polymerization of styrene are fairly low ($<10^6$) in the polymerization temperature range 60–90 °C. The general qualitative behavior of $\bar{D}$ is in agreement with the previous findings,[17] i.e., the collective diffusion coefficient at high concentrations goes through a maximum. At low concentrations, $\bar{D}$ is first due to the translational motions of individual polymer coils, and the concentration dependence of $\bar{D}$ is governed by $k_D$. The increase in $\bar{D}$ is then controlled by the presence of faster pseudogel motions[3] whose characteristic hydrodynamic screening length is relatively independent of molecular weight. Therefore, the maximum of $\bar{D}$ or the minimum of the screening length occurs at about the same

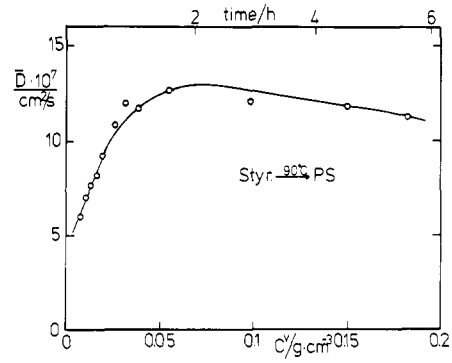


**Figure 22.** Plot of $\bar{D}$ ($\equiv\bar{\Gamma}/K^2$) vs. polymerization time and polystyrene concentration during the polymerization reaction at 90 °C.

concentrations for Figures 20–22.

In conclusion, we have demonstrated that unique surfaces can be constructed empirically for polymerization kinetics studies using a combination of light scattering and Raman spectroscopy. While the surfaces depend upon temperature and are modified by molecular weight distributions, the scheme offers an approach whereby we can monitor *on line* the molecular weight as well as the polymer concentration in a polymerization process. We have not yet investigated the effects of molecular weight polydispersity on the surfaces of Figures 1 and 12. However, unless the molecular weight distributions vary extensively during a polymerization process, the distortions on the surfaces can be viewed in the same manner as the overlap concentration $C^*$, the second virial coefficient $A_2$, or the radius of gyration $r_g$ is influenced by the molecular polydispersity effect.

**Acknowledgment.** B.C. thanks the U.S. Army Research Office for its continuous support of this research project and Dr. G. L. Hagnauer, AMMRC, Watertown, Mass., for his encouragements and helpful discussions.

## References and Notes

(1) de Gennes, P. G. "Scaling Concepts in Polymer Physics"; Cornell University Press: Ithaca, N.Y., 1979; p 324.
(2) Gulari, Erdogan; Gulari, Esin; Tsunashima, Y.; Chu, B. *Polymer* **1979**, *20*, 347.
(3) Chu, B.; Nose, T. *Macromolecules* **1979**, *12*, 599.
(4) Meeks, M.; Koenig, J. L. *J. Polym. Sci., Part A-2* **1971**, *9*, 717.
(5) Chu, B. "Laser Light Scattering"; Academic Press: New York, 1974.
(6) Nose, T.; Chu, B. *Macromolecules* **1979**, *12*, 590.
(7) Koppel, D. E. *J. Chem. Phys.* **1972**, *57*, 4814.
(8) Chu, B.; Gulari, Esin; Gulari, Erdogan *Phys. Scr.* **1979**, *19*, 476.
(9) Gulari, Esin; Gulari, Erdogan; Tsunashima, Y.; Chu, B. *J. Chem. Phys.* **1979**, *70*, 3965.
(10) Daoud, M.; Cotton, J. P.; Farnoux, B.; Jannink, G.; Sarma, G.; Benoit, H.; Duplessix, R.; Picot, C.; de Gennes, P. G. *Macromolecules* **1975**, *8*, 804.
(11) Adam, M.; Delsanti, M. *Macromolecules* **1977**, *10*, 1229.
(12) Nose, T.; Chu, B. *Macromolecules* **1979**, *12*, 1122.
(13) Chu, B.; Nose, T. *Macromolecules* **1980**, *13*, 122.
(14) Chu, B.; Fytas, G.; Zalczer, G. *Macromolecules* **1981**, *14*, 395.
(15) Abbey, K.; Kubota, K.; Chu, B. "NATO ASI Proceedings on Scattering Techniques"; Plenum Press: New York, 1981. Chu, B.; Kubota, K.; Abbey, K. M. *Polym. Prepr., Am. Chem. Soc., Div. Polym. Chem.* **1981**, *22*, 70.
(16) Tsunashima, Y.; Moro, K.; Chu, B. *Biopolymers* **1978**, *17*, 251.
(17) Patterson, G. D.; Stevens, J. R.; Alms, G. R.; Lindsey, C. P. *Macromolecules* **1979**, *12*, 658.